
PROBABILISTIC REGISTRATION FOR GAUSSIAN PROCESS 3D SHAPE MODELLING IN THE PRESENCE OF EXTENSIVE MISSING DATA *

Filipa Valdeira

Department of Environmental Science and Policy
Università Degli Studi di Milano
Milan
filipa.marreiros@unimi.it

Ricardo Ferreira

μ Robotics
Lisbon
alessandra.micheletti@unimi.it

Alessandra Micheletti

Department of Environmental Science and Policy
Università Degli Studi di Milano
Milan
alessandra.micheletti@unimi.it

Cláudia Soares

Computer Science Department, NOVA LINCS
NOVA School of Science and Technology, Universidade NOVA de Lisboa
Lisbon
claudia.soares@fct.unl.pt

ABSTRACT

Gaussian Processes are a powerful tool for shape modelling. While the existing methods on this area prove to work well for the general case of the human head, when looking at more detailed and deformed data, with a high prevalence of missing data, such as the ears, the results are not satisfactory. In order to overcome this, we formulate the shape fitting problem as a multi-annotator Gaussian Process Regression and establish a parallel with the standard probabilistic registration. The achieved method GPReg shows better performance when dealing with extensive areas of missing data when compared to a state-of-the-art registration method and the current approach for registration with GP.

Keywords Gaussian Processes · Shape modelling · Registration · Variational Bayes

1 Introduction

Consider the problem of predicting a complex 2D or 3D shape, like a human ear, from a dataset of similar point clouds and a few observed points of this shape. In this problem we face both the registration and modelling of different point clouds. There are increasing areas of application for 3D shape modelling, in particular, when it comes to human shape, spread over medical application (organ shape, segmentation, prosthesis design, surgical planning), surveillance (identity recognition, tracking) or human-machine interaction (face/expression recognition, gesture recognition, virtual humans) [5]. Most approaches focus on the human head, in particular on the face region, and great results have been achieved for coarse-grained models [4].

*This work has received funding from the European Union's Horizon 2020 research and innovation programme under the Marie Skłodowska-Curie Project BIGMATH, Grant Agreement No 812912.

However, small and detailed areas are still not accurately represented and this is the problem tackled in recent work [20]. Our driving example will be the modelling of an ear, representative of a fine-detailed region with extensive data problems, given the difficulty in data retrieval from a 3D scan procedure of the head: it presents extensive regions of missing data and a high level of noise. Our approach is nonetheless generic enough to be applied to any other shape as seen in Figure 4 of Section 5 with the 2D fish data.

A standard approach to obtain a shape model are 3D Morphable Models (3DMM), first proposed in [2]. Starting from raw point sets, they generally entail two main steps: *dense correspondence or registration*, expressing the correspondence between points of different scans according to their semantic meaning and *modelling*, expression of the shape variability in a lower dimension. Registration is by itself a broad area of study, that is usually considered separately from the modelling – a generic template shape is deformed to fit a target, without specific information on the shape characteristics. Therefore, initial approaches [2, 19] to 3DMM take an appropriate registration method and follow with Principal Component Analysis, to find a low-dimensional representation of shape variability.

In reality, however, most registration methods hide an implicit model that restricts the deformations allowed to the shapes. The main difference between model fitting and registration lies on the fact that, usually, restrictions to deformations are enforced by data in the former and by a regularization parameter in the latter. This means that, in higher level of abstraction, the process of registration is the same as model fitting.

We shall follow [12] to formalize the generic shape fitting problem. We consider a template shape $T = \{t_1, \dots, t_{N_T}\} \subset \mathbb{R}^d$ and a target shape $S = \{s_1, \dots, s_{N_S}\} \subset \mathbb{R}^d$, with possibly different number of points N_T and N_S . The former is a representative example of the shape being studied, as close as possible to any other shape, without missing data, outliers or noise, while the latter is any sample of the shape we have obtained. In previous work [23] with ear data scans, we have shown that the most part of the effects of translations and rotations can be previously removed; so it is here considered that the target and template were already preprocessed. Additionally, we want to introduce the scaling in the model, as this represents differences in size of the ears. Therefore, we only consider general non-rigid deformations between the template and a target shape, so that any residual rotation or translation, together with scaling, is taken into account by the deformations.

Therefore, we consider that a target is obtained from a template by applying a re-parametrization and a set of deformations θ . A re-parametrization is a diffeomorphism applied to a shape, ensuring that after its application each point of both shapes corresponds to the same feature/semantic meaning. As we are working in a discrete setting, we can represent this with a permutation matrix P . So, the problem is expressed as finding the optimal deformations between S and T

$$P^*, \theta^* \in \underset{P, \theta}{\operatorname{argmin}} d(\mathcal{T}(PT, \theta), S), \quad (1)$$

where $d(T, S)$ is a measure of dissimilarity quantifying the differences between two shapes and $\mathcal{T}(PT, \theta)$ is the transformed template after application of the deformations θ . The solution of Problem (1) provides a template whose points correspond to the points of the target, and are deformed to fit them. However, in practice, this problem is generally not solved in a unified manner. On the registration side, a generic constraint is applied to the deformations, while P is retrieved, not taking advantage of knowledge regarding the particular shape. On the shape fitting side, correspondence is often assumed (for example by previously applying a registration method) or retrieved in a trivial manner. Both of these options entail that the correspondence is obtained with a different model $\mathcal{T}(PT, \theta)$ than the fitting. Looking at the two processes in the same setting may be beneficial as it allows both of them to have more information, as stated in [14], where the authors propose a unified framework for shape modelling, based on Gaussian Processes (GP). The main idea is that prior assumptions on the shape structure can be incorporated independently from the registration algorithm, by building an appropriate kernel, so that the registration and shape fitting leverage the same model.

This framework has proven successful and has led to increasingly improved models of the human head [2, 21]. However, most efforts are made in terms of augmenting the data or generally improving model combination, i.e. how to bring together models originated from different datasets. When applying this process to 3D ear point clouds, we have observed that indeed this is the most promising approach [23], but it calls for an improved outlook on the registration procedure. When models of the full head are considered, ears are a small detail that is often overlooked or disregarded [2]. Therefore, a straightforward registration method is enough to provide a relatively good correspondence that leads to an overall good final model. The main difficulties of modelling the ear lie not only on the fine non-rigid deformations it presents, but also on the difficulty of data retrieval, due to its inherent anatomical shape, that lead to high occurrence of outliers and missing data. A recent work within the GP framework extends the head model with the ear [20]. Nonetheless, we note that the ear model in [20] requires the identification of 50 manual landmarks for registration. Besides, we approach the problem in a different way, aiming at first reconstructing the problematic ear data in the raw scans and then building the full model, while in [20] the head model is augmented with an ear model.

On the other hand, when looking at non-rigid registration methods we see increasingly better results through different approaches, but since they are usually decoupled from the modelling side, they do not allow for prior knowledge on the shape. This is usually only possible through a set of parameters restricting the amount of allowed deformation, but does not present the same freedom and convenience that modelling with kernels does. In fact, most regularization terms are equivalent to a Gaussian kernel and are not amenable to a different kernel formulation.

By modelling registration as a GP multi-annotator problem, we show that we can perform probabilistic registration within the GP framework, which allows us to benefit both from a complex prior through the kernels and from the nice properties of probabilistic assignment, particularly when dealing with outliers and noise.

1.0.1 Registration within the GP framework

Registration as an optimization problem In [14], the authors formulate the registration problem/model fitting for both surfaces and images. Here, we focus on the surface formulation. First, the authors do a low-rank approximation, obtaining a parametric approximation of the original kernel is. The problem is then posed as a Maximum a Posteriori (MAP) estimation problem, where the likelihood expresses some distance measure between the target and template shapes, and the prior is given by the GP. The authors chose the mean squared euclidean distance from the reference to the closest target point and solve the problem with an L-BFGS optimizer [13].

Non-rigid registration with ICP Another proposed approach to tackle the problem is a non-rigid application of the Iterative Closest Point, where the transformation part is obtained through Gaussian Process Regression (GPR). This means that to each point in the template we attribute the closest target point, based on their Euclidean distance. These correspondences are then taken as observations and GPR is used to compute deformations for the entire shape (the mean of the posterior is the template used in the next iteration). Our approach relates to this method, in the formulation of the problem but not in the way the correspondences are retrieved. For ear shapes, given the large regions of missing data and the highly non-rigid deformations, the closest point approach often leads to undesirable results [23].

1.0.2 Probabilistic registration

The previous approaches imply a deterministic attribution of correspondences between points, while a soft assignment may improve robustness to noise and outliers. This leads, in the registration area, to probabilistic registration methods, of which the most used and representative is the Coherent Point Drift (CPD) [18], that considers the alignment of two sets as a probability density estimation problem. This approach takes T (the template) as a set of centroids coming from a Gaussian Mixture Model (GMM) and S (the target) as points generated by the centroids. The transformation \mathcal{T} can be set as rigid, affine or non-rigid, producing 3 different versions of CPD; here, we are interested in its non-rigid formulation. An important detail is that the centroids are forced to move coherently as a group, thus preserving the topological structure of the points (motion coherence constraint over the velocity field). The goal is to find the most likely centroid from which each point in X was generated, thus resulting in a correspondence output. While considered state-of-the-art, CPD still presents some difficulties in overcoming high incidence of outliers, missing data and different number of points between the template and target. Consequently, variants of CPD have been developed in recent years to attempt to deal with such drawbacks by assigning different membership probabilities [16] or using k-connected neighbours [1] to enforce the preservation of local structure.

An interesting recent work [11] proposes a Bayesian Formulation of CPD (BCPD). Under this setting the authors guarantee convergence of the algorithm, introduce more interpretable parameters and reduce sensitivity to target rotation. Besides, this formulation is suitable to kernels other than the Gaussian one and so it has a close relationship with our work, although formulated in a different context. In fact, we will explore the parallel existing between BCPD and our approach under a set of assumptions, and we will also state why their differences make our approach more suitable for the problem at hand.

Interestingly, in [10] we see an improved version of BCPD, where GPR is used. However, we note that the introduction of GPs only has the purpose of accelerating the algorithm. The shapes are initially subsampled, after which a standard BCPD is conducted. The final step uses GPR to extend the obtained deformation to the full shape.

1.1 Our method

From the previous introduction and related work we conclude that proposals for registration within the GP framework target hard assignment and assume a one-to-one correspondence between the target and template, thus motivating their extension with a probabilistic assignment. An example of this can be seen in Figure 1. Several proposals for probabilistic methods exist in the registration area, but they generally do not consider extensive prior knowledge on the shape, other than imposing some regularization of the deformations, which usually can be translated to a Gaussian

kernel. This observation motivated us to develop a probabilistic registration method within the GP framework, where we can benefit both from a complex kernel prior and a soft assignment in the correspondences.

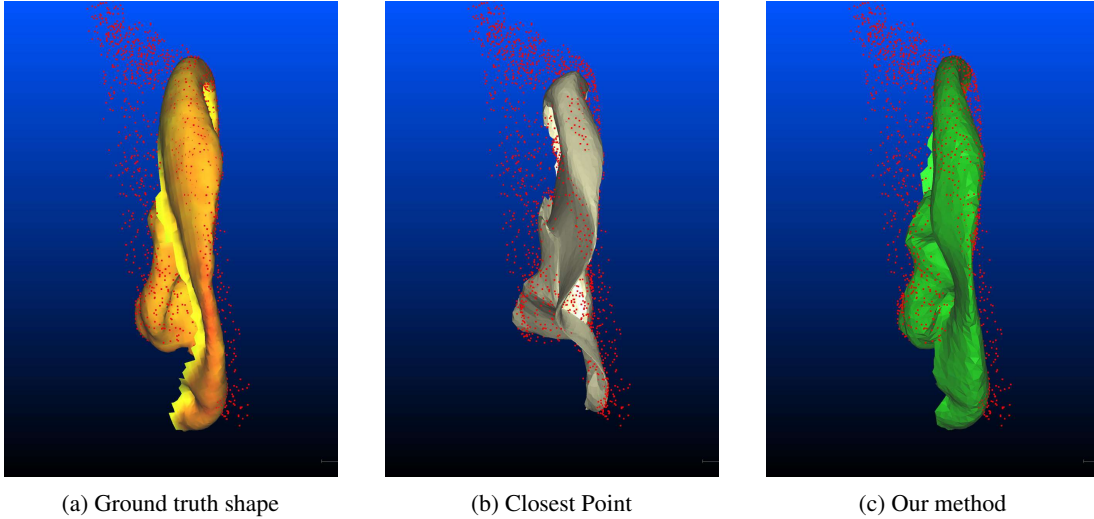


Figure 1: Lateral view of shape fitting for a 3D ear shape. On the left, we have the ground truth mesh in orange and the simulated ear as a point cloud in red, with noise, missing data and outliers. On the middle we have the result from the closest point approach and on the right the result with our method. We see that our result presents more resemblance to the original shape, specially in the areas with structured missing data (bottom of the shape).

Given the previous considerations we propose a new method, that bridges the gap between these two formulations. Our main contributions are:

- **Shape registration/model fitting as a multi-annotator GPR.** We show how the problem of registration with soft assignment can be understood within the GP framework as a multi-annotator Gaussian Process Regression (Section 3).
- **Parallel between probabilistic registration and our method, GPReg.** We provide a parallel between BCPD and our algorithm, under a few assumptions, which allows us to take advantage of the positive aspects of the probabilistic setting (Section 4). We further show how their differences lead to a good performance on the presence of extensive missing data (Section 5).
- **Application to a difficult registration problem – 3D ears registration.** We show that our method is suitable for the registration of 3D point clouds with highly non-rigid deformations, high occurrence of missing data and outliers, by performing simulations with 3D point sets of human ears. The results show improvement with respect to state-of-the-art registration methods and current GP registration proposals (Section 5).

2 Mathematical background

2.1 Gaussian Processes

Introduction to Gaussian Processes We refer to [22] for an introduction to the theory of Gaussian Processes. A Gaussian process (GP) is a collection of random variables, any finite number of which have a joint Gaussian distribution. A GP $f(x)$ is fully specified by its mean $\mu(x)$ and covariance function $k(x, x')$ defined as

$$\begin{aligned}\mu(x) &= \mathbb{E}[f(x)] \\ k(x, x') &= \mathbb{E}[(f(x) - \mu(x))(f(x') - \mu(x')))]\end{aligned}$$

and usually written as

$$f(x) \sim \mathcal{GP}(\mu(x), k(x, x')).$$

Gaussian Process Regression Given a dataset $\mathcal{D} = \{(x_i, y_i) \mid i = 1 \dots N\}$ of noisy observations $y_i \in \mathbb{R}^1$ for points $x_i \in \mathbb{R}^D$, we can model the observations as $y_i = f(x_i) + \epsilon$, where the noise follows an independent, identically distributed Gaussian distribution with zero mean and variance σ_n^2 and $f(x_i)$ is a GP. We further define matrix

$X = [x_1, \dots, x_N]$ and vector $y = [y_1, \dots, y_N]^T$. In this setting, the prediction of the response in correspondence of unobserved values $X_* = [x_1^*, \dots, x_p^*]$ can be obtained by Gaussian Process Regression (GPR). The predictive equations are found, with a Bayesian approach, to be [22]

$$f_* | X, y, X_* \sim \mathcal{N}(\bar{f}_*, \text{cov}(f_*)),$$

where

$$\begin{aligned} \bar{f}_* &= K_{X^*X} \left[K_{XX} + \sigma_n^2 I_N \right]^{-1} y \\ \text{cov}(f_*) &= K_{X^*X^*} - K_{X^*X} \left[K_{XX} + \sigma_n^2 I_N \right]^{-1} K_{XX^*}, \end{aligned} \quad (2)$$

where $K_{XX} = [k(x_i, x_i)]_{i=1}^N \in \mathbb{R}^{N \times N}$, $K_{X^*X} = [k(x_j^*, x_i)]_{j,i=1}^{P,N} \in \mathbb{R}^{P \times N}$, $K_{XX^*} = K_{X^*X}^T$, I_N is the identity matrix of size N and P is the number of unobserved values to be predicted.

GP for output in higher dimensions Gaussian processes are usually defined for scalar outputs y , but they can be extended to the vector-case under some assumptions, where the results obtained for the scalar case are still valid [9]. In particular, a useful class of covariance functions for the vector-valued case arises from the scalar-valued covariance functions [17]. Let $A \in \mathbb{R}^{d \times d}$ be a symmetric, positive definite matrix and l a real valued covariance function. It can be shown that the matrix valued function k with entries k_{ij} defined by $k_{ij} = A_{ij}l(x, y)$ is a valid covariance, with A_{ij} representing the correlation between the i -th and j -th output component. Therefore, if we assume that different dimensions have no correlation, we can use a scalar kernel and set A as the identity matrix, so any existing kernel can be employed in this setting.

2.1.1 GPR with multiple annotators

In learning from data it is often seen that there are no given exact labels for the data (e.g. the attribution of a label is subjective and so there is no exact ground truth). A common approach is to obtain a collection of labels for each data point, provided by different annotators, with different levels of confidence. A proposal for GPR with multiple labels is given in [8]. Instead of $\mathcal{D} = \{(x_i, y_i) | i = 1, \dots, N\}$, we consider a collection $\mathcal{D}_m = \{(x_i^m, y_i^m) | i = 1, \dots, N_m\} = (X_m, y_m)$ of the m -th annotator. We further define $X = \cup_{m=1}^M X_m$ and $Y = \{y_1, \dots, y_M\}$ and N remains the number of unique inputs in X (each annotators does not necessarily provide a label for all unique input points).

So, for each unique $x_i \in X$, we compute the associated variance and label as a combination of all annotators in the following way

$$\frac{1}{\hat{\sigma}_i^2} = \sum_{m \sim i} \frac{1}{\sigma_m^2}, \quad \hat{y}_i = \hat{\sigma}_i^2 \sum_{m \sim i} \frac{y_i^m}{\sigma_m^2}, \quad (3)$$

where $m \sim i$ stands for all m annotations retrieved for data point i and σ_m^2 is the variance associated to the m -th annotator. Assuming annotators provide the labels independently from each other we have that

$$p(Y|f) = \prod_m \prod_{i \sim m} \mathcal{N}(y_i^m | f_i, \sigma_m^2),$$

and so the posterior $p(f|Y)$ follows a Gaussian distribution $\mathcal{N}(\mu_p, \Sigma_p)$, with mean and covariance

$$\begin{aligned} \mu_p &= (K^{-1} + \hat{\Sigma}^{-1})^{-1} \hat{\Sigma}^{-1} \hat{y} \\ \Sigma_p &= (K^{-1} + \hat{\Sigma}^{-1})^{-1}, \end{aligned}$$

where $\hat{\Sigma} = \text{diag}(\hat{\sigma}_1^2, \dots, \hat{\sigma}_N^2)$ and $\hat{y} = [\hat{y}_1, \dots, \hat{y}_N]^T$, with $\hat{\sigma}_i^2$ and \hat{y}_i are given by (3). Therefore, the predictive equations can be obtained as

$$\begin{aligned} \bar{f}_* &= K_{X^*X} (K_{XX} + \hat{\Sigma})^{-1} \hat{y} \\ \text{cov}(f_*) &= K_{X^*X^*} - K_{X^*X} (K_{XX} + \hat{\Sigma})^{-1} K_{XX^*}, \end{aligned} \quad (4)$$

where the kernel matrices are defined in (2). We can see that these equations differ from (2) only on the noise covariance matrix and label vector, but follow the exact same structure.

2.2 Probabilistic shape registration

We will briefly introduce the framework of probabilistic registration, following the Bayesian formulation in [11]. The main idea behind this line of work is that the template (T), upon an appropriate transformation, can be seen as centroids of a Gaussian Mixture Model, where target points of any shape (S) are data generated by the centroids. Further, a point s_j can be an outlier with probability ω , in which case it is generated from an outlier probability $p_{out}(s_j)$. If s_j is not an outlier, then it corresponds to point y_m with probability α_m – membership probability.

In [11] the authors consider explicit similarity transformations and non-rigid ones, such that a point i of the transformed template is given as

$$\mathcal{T}(t_i) = sR(t_i + \delta_i) + p, \quad (5)$$

where s is a scale factor, R is a rotation matrix, p is a translation vector and δ_i is a displacement vector for non-rigid transformations. According to GMM, the generation of a target point s_j follows a multivariate normal distribution with mean $\mathcal{T}(t_i)$ – the transformed template point – and covariance matrix $\varsigma^2 I_d$, so

$$\phi_{ij}(s_j; \mathcal{T}(t_i), \varsigma^2) = \frac{1}{(\varsigma\sqrt{2\pi})^d} \exp\left(-\frac{\|s_j - \mathcal{T}(t_i)\|^2}{2\varsigma^2}\right). \quad (6)$$

In order to explicitly introduce correspondences, two additional variables are added: $c \in \{0, 1\}^{N_S}$, an indicator variable that takes value of 1 for c_j if point s_j is an outlier, and $e \in \{1, \dots, N_T\}^{N_S}$, where $e_j = i$ if the j -th target point corresponds to the i -th template point. Taking the assumptions regarding outliers into account, we have the joint distribution for (x_j, e_j, c_j) as

$$p(s_j, e_j, c_j | T, \delta, \sigma^2) = \{wp_{out}(s_j)\}^{1-c_j} \left\{ (1-w) \prod_{i=1}^{N_T} (\alpha_i \phi_{ij})^{\gamma_i(e_j)} \right\}^{c_j}, \quad (7)$$

where γ_i is an indicator function, taking a value of 1 if $e_j = i$ and 0 otherwise, and α_i is the probability that $e_j = i$, with $\sum_{i=1}^{N_T} \alpha_i = 1$. The authors take $p(\alpha)$ as a Dirichlet distribution and set a prior on the deformations as

$$p(\delta | T) = \phi(\delta; 0, \lambda^{-1} G \otimes I_d),$$

where $G = (g_{ii'}) \in \mathbb{R}^{N_T \times N_T}$, with $g_{ii'} = k(i, i')$, and λ is a positive constant.

Finally, the full joint is given as

$$p(S, T, \theta) \propto p(\delta | T) p(\alpha) \prod_{j=1}^{N_S} p(s_j, e_j, c_j | T, \delta, \varsigma^2, \alpha, \rho), \quad (8)$$

where $\theta = (v, \varsigma^2, \alpha, \rho, c, e)$ and $\rho = (s, R, p)$.

3 GP shape registration with multi-annotators

In this section we present the formulation of our problem within the GP framework, following the approach in [14]. For a visual representation of the described model, we refer the reader to the respective graphical model in Figure 2.

3.1 Problem formulation and notation

We consider that any shape $S = \{s_1, \dots, s_{N_S}\}$ can be obtained from a template shape $T = \{t_1, \dots, t_{N_T}\} \subset \mathbb{R}^d$, where $s_i, t_i \in \mathbb{R}^d$. We assume that we can obtain S by adding deformations $u(t)$ to the template points, where $u(t)$ are modelled as a Gaussian Process defined by a mean function $\mu : \mathbb{R}^d \rightarrow \mathbb{R}^d$ and a kernel $K : \mathbb{R}^d \times \mathbb{R}^d \rightarrow \mathbb{R}^{d \times d}$, so $u(t) \sim GP(\mu(t), K(t, t'))$.

Note that we are working in the case of non-scalar output, but as stated above we can apply the same result as long as we ensure that the kernel used is a valid one. Therefore, we will mostly work with vector representations of both target and template. This means that one observation consists of a single component of a point, we can then choose between introducing dependency between components based on the choice of kernel.

We further assume that we can get noisy observations of the deformations $\delta(t) = u(t) + \epsilon$, where $\epsilon \sim \mathcal{N}(0, \sigma_n^2)$. With these assumptions, we can see that we lie in the GP framework introduced in Section 2.1, where the template points t_i correspond to the points x_i , the observed deformations $\delta(t_i)$ correspond to the observations y_i and the true deformations $\mu(t)$ to the function $f(x)$, the GP.

Modelling missing data and outliers In [14] the authors assume a one-to-one correspondence between target and template, so each target point can be obtained from a template point with a deformation, $S = \{t + u(t) | t \in T\}$. As we have seen, this is often not the case for real data. Therefore, we consider that there are both missing data and outliers in our target shapes and so there are points of the template without correspondence in the target and vice-versa. We formulate this assumption by splitting the template T into two subsets $\{T_{corr}, T_{miss}\}$, where the former set contains the points with correspondence and the latter the ones with missing data. In the same way, we split S into the corresponding points and outliers, $S = \{S_{corr}, S_{out}\}$, such that S_{corr} is in correspondence with T_{corr} . So, for each point of T_{corr} we observe the following deformations

$$\delta = \begin{bmatrix} \delta_{C_1} \\ \vdots \\ \delta_{C_C} \end{bmatrix} = \begin{bmatrix} s_{t_{C_1}} - t_{C_1} \\ \vdots \\ s_{t_{C_C}} - t_{C_C} \end{bmatrix}, \quad (9)$$

where $T_{corr} = \{t_{C_1}, \dots, t_{C_C}\}$ and $s_{t_{C_i}}$ is the target point corresponding to the template point t_{C_i} .

3.1.1 Notation

We will use the following notation from this section onwards

- $S = \{s_1, \dots, s_{N_S}\} \subset \mathbb{R}^d$ – the target shape point set, with its respective vector representation $s = (s_1^T, \dots, s_{N_S}^T)^T \in \mathbb{R}^{N_S d}$
- $T = \{t_1, \dots, t_{N_T}\} \subset \mathbb{R}^d$ – the template shape point set, with its respective vector representation $t = (t_1^T, \dots, t_{N_T}^T)^T \in \mathbb{R}^{N_T d}$
- $T_{corr} = \{t_{C_1}, \dots, t_{C_C}\}$ – set of template points with correspondence to target, where C is the number of points with correspondence
- $S_{corr} = \{s_{t_{C_1}}, \dots, s_{t_{C_C}}\}$ – set of target points with correspondence to template, where $s_{t_{C_i}}$ is the target point corresponding to the template point t_{C_i}
- $\Delta = \{\delta_{C_1}, \dots, \delta_{C_C}\} \subset \mathbb{R}^d$ – the deformations for each template point with correspondence, with its respective vector representation $\delta = (\delta_{C_1}^T, \dots, \delta_{C_C}^T)^T \in \mathbb{R}^{N_T d}$
- $D_{\sigma_n^2} = \text{diag}(\sigma_{C_1}^2, \dots, \sigma_{C_C}^2)$ – diagonal matrix of observation noise, where $\sigma_{C_i}^2$ is the variance of noise for observed deformation δ_{C_i}
- $C_i = \{j : s_j \in S, p_{i,j} > P_{MIN}\}$ – set of indices of target shape with correspondence with template point t_i
- $K = K_{TT} = (k(t_i, t_i))_{i=1}^{N_T} \in \mathbb{R}^{N_T d \times N_T d}$ – the kernel matrix of the entire template point set
- $K_{T_{corr}T_{corr}} = (k(t_{C_i}, t_{C_i}))_{i=1}^C \in \mathbb{R}^{C d \times C d}$ – the kernel matrix of the template points with correspondence
- I_d – the identity matrix of size d
- ω – outlier probability
- $D_{\zeta^2} = \text{diag}(\zeta_1^2, \dots, \zeta_{N_T}^2)$ – the diagonal matrix of registration noise, where ζ_i^2 is the variance associated to template point t_i
- $\tilde{A} = A \otimes I_d$ – the Kronecker product of matrix A with I_d
- $\mathbf{1}_N$ – the vector of ones with size N

3.1.2 Formulation of the registration problem

Within this framework, and because of the gaussianity of the distributions, for which the mode and mean coincide, the shape fitting and registration problem is usually formulated as a MAP problem [15], that is

$$\underset{u}{\operatorname{argmax}} p(u|T, S).$$

In particular, for our case, it depends on the observed points and deformations, so we have

$$\underset{u}{\operatorname{argmax}} p(u|T_{corr}, \delta).$$

However, we do not know the correspondence beforehand, so T_{corr} , δ are not known and they also depend on u , leading to

$$\underset{u}{\operatorname{argmax}} p(u|T_{corr}(u), \delta(u)). \quad (10)$$

In an ICP-like approach we split our problem into two, where we keep u fixed in the inner maximization and T_{corr}, δ fixed in the outer. So, our final formulation is

$$\max_u \left\{ \max_{T_{corr}, \delta} p(u | T_{corr}(u), \delta(u)) \right\}. \quad (11)$$

In the outer optimization we are computing the transformation given the current correspondences and in the inner cycle we are computing the correspondences given the current deformation of the template.

3.2 Formulation with multi-annotators

3.2.1 With hard assignment

Let us first consider the case where we take a single correspondence for the template inliers. In this situation, we will have a vector δ of observed deformations corresponding to each point in the set T_{corr} . For fixed T_{corr}, δ we are interested in the MAP of the GP posterior, which corresponds to the mean in the prediction equations of GPR (2). Applying (2) to all points in the template, yields $\delta^* | T, T_{corr}, \delta \sim \mathcal{N}(\mu_p, D_{\sigma_p}^2)$, where $\mu_p \in \mathbb{R}^{N_T d}$, $D_{\sigma_p}^2 \in \mathbb{R}^{N_T d \times N_T d}$ are given as

$$\begin{aligned} \mu_p &= K_{T_{corr}T}^T (K_{T_{corr}T_{corr}} + D_{\sigma_n}^2)^{-1} \delta \\ D_{\sigma_p}^2 &= K_{TT} - K_{T_{corr}T}^T (K_{T_{corr}T_{corr}} + D_{\sigma_n}^2)^{-1} K_{T_{corr}T}, \end{aligned} \quad (12)$$

where $D_{\sigma_n}^2 = \text{diag}(\sigma_{C_1}^2, \dots, \sigma_{C_C}^2)$ is the diagonal matrix expressing the noise associated to each observation (assumed known for the time being). The deformed template is then obtained as $\tilde{t} = t + \mu_p$, to be used in the inner iteration for computation of the correspondences.

Remark on the kernel matrices. Note that we are working in a discrete setting and this is why we can express μ_p and $D_{\sigma_p}^2$ as a vector and a matrix instead of functions. This is because we are working in the template point set and we are only interested in predictions at those points. We also note that K_{TT} , the kernel matrix of all template points, is constant and that all other kernel matrices ($K_{T_{corr}T_{corr}}$, $K_{T_{corr}T}$) are subsets of it. Therefore, we note K_{TT} simply as K .

3.2.2 Introducing soft-assignment with multi-annotators

Introduce a soft-assignment means to attribute different possible target points to each template point, each with a different probability of correspondence. We can interpret this as each template point having several different possible labels (deformations) given by annotators with different levels of confidence (probability of correspondence). Therefore, one point t_i will have N_S labels corresponding to each point in the target that could be a possible match.

We are now in the setting of GP with multi-annotators, introduced in Section 2.1.1. As we have seen, the predictive equations for GPR remain the same with a different noise covariance matrix and observations vector, as these are built from the multiple labels, according to (3). In the context of our problem, the equations become

$$\frac{1}{\sigma_{C_i}^2} = \sum_{j \in \mathcal{C}_i} \frac{1}{(\sigma_{C_i}^j)^2} \quad \delta_{C_i} = \sigma_{C_i}^2 \sum_{j \in \mathcal{C}_i} \frac{\delta_{C_i}^j}{(\sigma_{C_i}^j)^2}, \quad (13)$$

where $\delta_{C_i}^j = s_j - t_{C_i}$. The variance $(\sigma_{C_i}^j)^2$, corresponding to the annotator's confidence in the original formulation, represents here the probability of correspondence between point C_i and m . Note that while the variance of annotator j was the same across the data points i in the original formulation, here we consider that annotator j of point C_i is not necessarily the same as annotator j of point C_k , i.e. there can be at most $N_T \times N_S$ annotators.

In order to complete our algorithm, two points need to be addressed: how to define the correspondence set T_{corr} and how to compute $(\sigma_{C_i}^j)^2$. The computation of this value will be detailed in the next section.

4 Computation of variance

In order to obtain a theoretically sound update for elements $\sigma_{C_i}^j$ in (13) we first reformulate our problem in the standard probabilistic approach as introduced in Section 2.2. Then, we establish a parallel with the BCPD framework. In this derivation we follow the Bayesian formulation proposed in [11], instead of the original in [18].

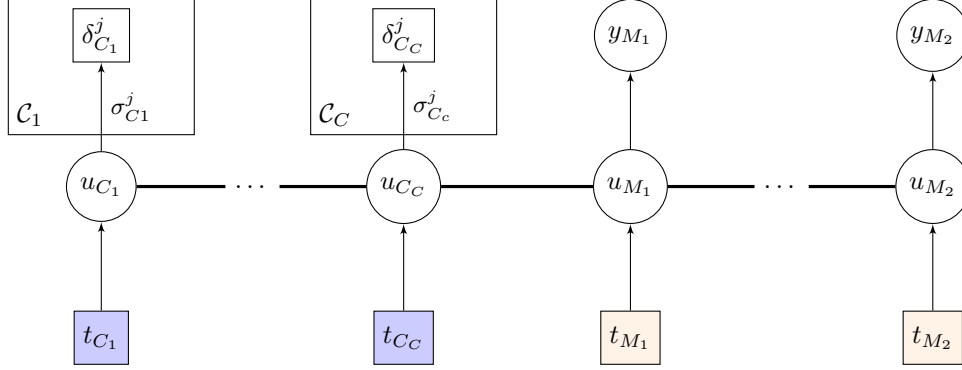


Figure 2: Graphical model for the GP with multiple annotators in the context of shape modelling. Squared nodes represent observed variables and circles are latent ones. Templates points with correspondence are identified with blue, while missing points are identified with orange.

4.1 Formulation

We will briefly detail the assumptions and problem formulation used in this approach, by deriving equivalents of equations (5) through (8) according to our assumptions. This will lead to the final expression for the joint distribution in (17).

Transformation model We do not consider similarity transformations, so the transformation acting on the template is merely given by a displacement vector δ_i

$$\mathcal{T}_i = t_i + \delta_i. \quad (14)$$

Gaussian mixture model According to the GMM we obtain a similar expression to (6)

$$\phi_{ij}(s_j; \bar{t}_i, \varsigma_i^2) = \frac{1}{(\varsigma_i \sqrt{2\pi})^d} \exp\left(-\frac{\|s_j - \mathcal{T}_i\|^2}{2\varsigma_i^2}\right), \quad (15)$$

but we introduce an individual variance for each template point given as ς_i^2 . As we will show later, this has a positive impact when dealing with large regions of missing data. With respect to the outliers, we follow the same assumptions as in BCPD, but for simplification we take $p_{out}(s_j) = 1/N_S$, as was previously taken in CPD. Besides, we take equal membership probabilities $\alpha_i = 1/N_T$, meaning that a point in the target is expected to belong to any point of the template with equal probability. This is also the assumption in CPD and is here taken for simplification on this first formulation of the framework. Thus, we obtain the joint distribution

$$p(s_j, e_j, c_j | T, \delta, \sigma^2) = \left\{ \frac{w}{N_S} \right\}^{1-c_j} \left\{ \frac{(1-w)}{N_T} \prod_{i=1}^{N_T} (\phi_{ij})^{\gamma_i(e_j)} \right\}^{c_j}. \quad (16)$$

Prior distributions The prior on the deformations is expressed with the previously defined kernel K , but we take $\lambda = 1$, as we can usually include this parameter as part of the kernel estimation. We then have the prior given as $p(\delta|t) = \mathcal{N}(0, K)$.

4.1.1 Full joint distribution

Finally, the full joint distribution is given as

$$p(s, t, \theta) \propto p(\delta|t) \prod_{j=1}^{N_S} p(s_j, e_j, c_j | t, \delta, \varsigma^2), \quad (17)$$

where $\theta = (\delta, \varsigma^2, c, e)$ are the parameters to be estimated.

4.2 Solving the problem with Variational Bayesian Inference

We will estimate the parameters θ in (17) using Variational Bayesian Inference (VBI) [3], a tool often employed when dealing with challenging posterior distributions. We start by providing an overview on VBI and how it can be employed for our problem, followed by the update equations obtained through this approach.

4.2.1 Introduction

The idea behind VBI is to use a distribution $q(\theta)$ to approximate the posterior $p(\theta|S, T)$ and then minimize the Kullback–Leibler (KL) divergence between them

$$\begin{aligned} q^*(\theta) &= \operatorname{argmin}_{q(\theta \in Q)} KL(q(\theta) \parallel p(\theta|S, T)) \\ &= \operatorname{argmin}_{q(\theta \in Q)} \mathbb{E}[\log q(\theta)] + \mathbb{E}[\log p(\theta, T, S)] + \log p(S, T), \end{aligned}$$

where Q is a predefined set of distribution families to which q belongs. However, as the $\log p(S, T)$ may not be computable, the evidence lower bound (ELBO) is maximized instead

$$ELBO(q) = \mathbb{E}[\log p(\theta, T, S)] - \mathbb{E}[\log q(\theta)].$$

. The ELBO is equivalent to the negative KL divergence up to a constant, and therefore maximizing the former is equivalent to minimizing the latter. One possible family is the mean-field variational family, where the latent variables are mutually independent and governed by different factors – it is the one we pick here, so $q(\theta) = \prod_{i=1}^M q_i(\theta_i)$. In particular, we will consider

$$q(\theta) = q_1(\delta)q_2(c, e)q_{31}(\zeta_1^2)\dots q_{3i}(\zeta_i^2)\dots q_{31}(\zeta_{N_T}^2).$$

A standard method to maximize the ELBO, and the one followed here, is the Coordinate Ascent Mean-field VI. If we fix all other q_j , then we know that optimal q_i is

$$q_i(\theta_i)^* \propto \exp\{\mathbb{E}_{-i}[\log p(\theta_i|\theta_{-i}, S, T)]\} \propto \exp\{\mathbb{E}_{-i}[\log p(\theta_i, \theta_{-i}, S, T)]\}, \quad (18)$$

where $\mathbb{E}_{-i}[\log p(\theta, S, T)]$ is the expectation of the joint probability with respect to the remaining $q_{j \neq i}$ and θ_{-i} corresponds to all parameters in θ except θ_i . So, each q_i is updated iteratively by computing $\mathbb{E}_{-i}[\log p(\theta, S, T)]$, until convergence is reached. Note that at each step we will need the expected value of the remaining variables. Further, at each step we are updating the distribution parameters of q_i .

4.2.2 Update equations

We present the updates for each component in Proposition 1, Proposition 2 and Proposition 3. The derivations closely follow the ones in [11] and can be found in Supplementary Material. In general, the final equations exhibit a similar structure except that ζ^2 , taken as a scalar in [11], is replaced by the diagonal matrix D_{ζ_i} .

For ease of notation, and in preparation for the subsequent equations, we define $p_{ij} = E[c_j \gamma_i(e_j)]$ as the probability of correspondence between template point i and target point j , with the respective probability matrix $P = (p_{ij}) \in [0, 1]^{N_T \times N_S}$. We further define $\nu_i = \sum_{j=1}^{N_S} p_{ij}$, representing the expected number of target points corresponding with t_i , as well as $\nu = P \mathbf{1}_{N_S}$, the corresponding vector.

Proposition 1. *The update equations for the expected value and covariance of δ are found to be*

$$\begin{aligned} E[\delta] &= \Sigma \tilde{D}_\nu \tilde{D}_{\zeta^2}^{-1} (\tilde{D}_\nu^{-1} \tilde{P} s - t) \\ \operatorname{Cov}(\delta) &= \Sigma = (K^{-1} + \tilde{D}_\nu \tilde{D}_{\zeta^2}^{-1})^{-1}, \end{aligned} \quad (19)$$

where $D_{\zeta^2} = \operatorname{diag}(\zeta_1^2, \dots, \zeta_{N_T}^2)$ and $D_\nu = \operatorname{diag}(\nu_1, \dots, \nu_{N_T})$.

Proposition 2. *The update for the correspondence probability is found to be*

$$p_{ij} = \frac{(1-w)\langle \phi_{ij} \rangle}{\frac{N_T}{N_S} w + (1-w) \sum_{i'=1}^{N_T} \langle \phi_{i'j} \rangle}, \quad (20)$$

where $\langle \phi_{ij} \rangle = \phi_{ij}(s_j; \bar{t}_i, \zeta_i^2) \exp\left\{-\frac{\operatorname{Tr}(\operatorname{Cov}(\delta_i))}{2\zeta_i^2}\right\}$ and $\bar{t}_i = E[\mathcal{T}_i] = t_i + E[\delta_i]$.

Proposition 3. *The update for each variance term ζ_i^2 is given as*

$$\zeta_i^2 = \frac{1}{d} \left(\frac{[\tilde{P} \operatorname{diag}(s)]_i - 2\bar{t}_i^T [\tilde{P} s]_i}{\nu_i} + \|\bar{t}_i\|^2 + \operatorname{Tr}(\operatorname{Cov}(\delta_i)) \right). \quad (21)$$

4.3 Parallel with GP framework

If consider no missing points in our formulation then it is possible to establish a parallel with this framework. For this we reformulate our expressions in order to obtain a similar struture to the ones in the previous section. Note that the update step of p_{ij} can be understood as the getting correspondence part, so the inner optimization.

Proposition 4. *Considering no missing points, i.e. $T_{corr} = T$, and if the variance $(\sigma_{C_i}^j)^2$ in equation (13) is taken as*

$$(\sigma_{C_i}^j)^2 = \frac{\zeta_i^2}{p_{ij}}, \quad (22)$$

where p_{ij} is given by (20), then a parallel exists between the update equations in Proposition 1, Proposition 2, Proposition 3 and the update equations for multi-annotator GPR in (12).

Proof. When $T_{corr} = T$, and since $K^T = K$, the posterior mean and covariance in (12) become

$$\begin{aligned} \mu_p &= K(K + \tilde{D}_{\sigma_n^2})^{-1}\delta \\ D_{\sigma_p^2} &= K - K(K + \tilde{D}_{\sigma_n^2})^{-1}K, \end{aligned}$$

where $D_{\sigma_n^2} = \text{diag}(\sigma_1^2, \dots, \sigma_{N_T}^2)$, with σ_i^2 and δ_i given by (13) and here restated without the notation for correspondences

$$\frac{1}{\sigma_i^2} = \sum_{j \in N_S} \frac{1}{(\sigma_i^j)^2} \quad \delta_i = \sigma_i^2 \sum_{j \in N_S} \frac{\delta_i^j}{(\sigma_i^j)^2}.$$

Taking the variance as in (22), we can write the previous equations as

$$\begin{aligned} \frac{1}{\sigma_i^2} &= \frac{P_i \mathbf{1}_{N_S}}{\zeta_i^2} = \frac{\nu_i}{\zeta_i^2} \\ \delta_i &= \nu_i^{-1} \sum_j p_{ij}(s_j - t_i) = \nu_i^{-1} \tilde{P}_i s - \nu_i^{-1} \sum_j p_{ij} t_i = \nu_i^{-1} \tilde{P}_i s - t_i, \end{aligned}$$

where P_i refers to the i -th row of matrix P . Therefore, we have that $D_{\sigma_n^2} = D_{\zeta^2} D_\nu^{-1}$ and $\delta = \tilde{D}_\nu^{-1} \tilde{P} s - t$. The posterior deformations in (4.3) can then be written as

$$\begin{aligned} \mu_p &= K(K + \tilde{D}_{\zeta^2} \tilde{D}_\nu^{-1})^{-1}\delta \\ &= KK^{-1} \left[\mathbf{1} + \tilde{D}_{\zeta^2} \tilde{D}_\nu^{-1} K^{-1} \right]^{-1} \delta \\ &= \left[K^{-1} + \tilde{D}_\nu \tilde{D}_{\zeta^2}^{-1} \right]^{-1} \tilde{D}_\nu \tilde{D}_{\zeta^2}^{-1} (\tilde{D}_\nu^{-1} \tilde{P} s - t) \end{aligned}$$

and the covariance as

$$\begin{aligned} D_{\sigma_p^2} &= K - K(K + \tilde{D}_{\zeta^2} \tilde{D}_\nu^{-1})^{-1}K \\ &= K - \left[K^{-1} + \tilde{D}_\nu \tilde{D}_{\zeta^2}^{-1} \right]^{-1} \tilde{D}_\nu \tilde{D}_{\zeta^2}^{-1} K \\ &= \left[K^{-1} + D_\nu D_{\zeta^2}^{-1} \right]^{-1} \left[K(K^{-1} + \tilde{D}_\nu \tilde{D}_{\zeta^2}^{-1}) - \tilde{D}_\nu \tilde{D}_{\zeta^2}^{-1} K \right] \\ &= \left[K^{-1} + \tilde{D}_\nu \tilde{D}_{\zeta^2}^{-1} \right]^{-1}, \end{aligned}$$

thus being equivalent to the expressions for $\mathbb{E}[\delta]$ and $\text{Cov}(\delta)$ in (19). So if we follow the update for p_{ij} and ζ_i^2 according to Proposition 2 and Proposition 3 and we have a full parallel in the update steps. \square

Although this is established for the case of no missing data, we take (22) as a reasonable update for the annotators variance, together with the necessary updates for p_{ij} and ζ_i^2 .

4.4 Missing data points

Given the probability matrix P , we apply a predefined threshold P_{MIN} , such that pairings with a lower value than P_{MIN} are considered as non-corresponding. So, for each point t_i , the considered correspondences to the target are $\mathcal{C}_i = \{j : s_j \in S, p_{ij} > P_{MIN}\}$. Then if a point t_i has no elements in \mathcal{C}_i , it is considered a missing point, meaning that $T_{miss} = \{t_i : t_i \in T, |\mathcal{C}_i| = 0\}$ and $T_{corr} = \{t_i : t_i \in T, |\mathcal{C}_i| > 0\}$.

4.5 Final algorithm

We present the pseudo-code for our method in Algorithm 1 and Algorithm 2, where the former contains the main outer steps and the latter details the computation for the correspondence part.

Algorithm 1 Registration

Input: $t, s, K, D_{\zeta^2}, \omega, P_{MIN}$

- 1: $\bar{t} = t$
- 2: **while** some stopping criterion is not met **do**
- 3: $T_{corr}, \delta, D_{\sigma_n^2} = \text{get_correspondences}(t, s, \bar{t}, D_{\sigma_p^2}, D_{\zeta^2}, \omega, P_{MIN})$
- 4: $\mu_p = K_{T_{corr}T}^T (K_{T_{corr}T_{corr}} + \tilde{D}_{\sigma_n^2})^{-1} \delta$
- 5: $D_{\sigma_p^2} = K_{TT} - K_{T_{corr}T}^T (K_{T_{corr}T_{corr}} + \tilde{D}_{\sigma_n^2})^{-1} K_{T_{corr}T}$
- 6: $\bar{t} = t + \mu_p$
- 7: $\zeta_i^2 = \frac{1}{d} \left(\frac{[\tilde{P} \text{diag}(s)]_i - 2\bar{t}_i^T [\tilde{P}s]_i}{\nu_i} + \|\bar{t}_i\|^2 + \text{Tr}(\text{Cov}(\delta_i)) \right)$
- 8: **end while**

Algorithm 2 get_correspondences

Input: $t, s, \bar{t}, D_{\sigma_p^2}, D_{\zeta^2}, \omega, P_{MIN}$

Output: $D_{\sigma_n^2} = \text{diag}(\sigma_{C_1}^2, \dots, \sigma_{C_C}^2), \delta = (\delta_{C_1}^T, \dots, \delta_{C_C}^T)^T, T_{corr}$

- 1: **for** $(i, j) \leftarrow (1, 1)$ to (N_T, N_S) **do**
- 2: $\phi_{ij}(s_j; \bar{t}_i, \zeta^2) = \frac{1}{(\zeta_i \sqrt{2\pi})^d} \exp\left(-\frac{\|s_j - \bar{t}_i\|^2}{2\zeta_i^2}\right)$
- 3: $\langle \phi_{ij} \rangle = \phi_{ij} \exp\left\{-\frac{1}{2\zeta^2} \text{Tr}(\sigma_{P_i}^2 I_d)\right\}$
- 4: $p_{ij} = \frac{(1-w)\langle \phi_{ij} \rangle}{\frac{N_T}{N_S} w + (1-w) \sum_{i'=1}^{N_T} \langle \phi_{i'j} \rangle}$
- 5: $(\sigma_i^j)^2 = \frac{\zeta_i^2}{p_{ij}}$
- 6: **end for**
- 7: $C_i = \{j : s_j \in S, p_{ij} > P_{MIN}\}$
 $T_{corr} = \{t_i : t_i \in T, |C_i| > 0\}$
- 8: **for** $i \in T_{corr}$ **do**
- 9: $\frac{1}{\sigma_{C_i}^2} = \sum_{j \in C_i} \frac{1}{(\sigma_{C_i}^j)^2}$
- 10: $\delta_{C_i} = \sigma_{C_i}^2 \sum_{j \in C_i} \frac{\delta_{C_i}^j}{(\sigma_{C_i}^j)^2}$
- 11: **end for**

5 Experimental results and discussion

5.1 2D data

5.1.1 Dataset

As 2D data we take the Fish dataset [6], where the template is a 2D fish with 98 points. The target point sets are then generated by applying different kinds of alterations to the data. Non-rigid deformations are generated by warping the template points with a Gaussian radial basis function. The dataset has four other variations considering outliers, missing data, rotation and noise, all of them with a moderate level of deformations included. In order to accurately replicate the ear data challenges, we further create a new dataset, based on the noise level 2 of the Fish dataset. Here, we introduce structured missing data in the following way: we choose one point of the template as centre and increasingly set the width of a squared bounding box around this point — all the points within the box are removed. We consider different locations of this centre to get representative results.

5.1.2 Setting

We consider different variations of our method, as well as different variations of BCPD, in order to show the relevance of the introduced modifications. Therefore, we will denote

- *GPReg_Full* - our proposed method in its complete version;
- *GPReg_bcpdReg* - our proposed method where the registration variance ζ^2 is taken as a scalar instead of a vector;
- *GPReg_noTresh* - our proposed method without the threshold for missing points P_{MIN}
- *GPClosestPnt* - registration with GPR, but where the correspondence part is achieved by taking the closest point, i.e. not considering multi-annotators;
- *BCPD_Standard* - BCPD method with the suggested parameters from the authors;
- *BCPD_Opt_Norm* - BCPD method with optimized parameters for the Fish dataset (conducted by grid search), with normalization of both shapes;
- *BCPD_Opt_noNorm* - BCPD method with optimized parameters for the Fish dataset (conducted by grid search), without normalization of both shapes, since this is not used in our method and could potentially benefit it in some cases. (By no normalization, we mean that shapes maintain their relative size. They are actually both normalized with respect to the target shapes, as recommended by BCPD authors.)

To fairly compare our method with BCPD, we set their parameters in the same way whenever possible — consequently, we will use the Squared Exponential kernel for our model. The remaining parameters are tuned with the deformation level 1 for both methods, by grid search. A detailed description of all settings can be found in Supplementary material.

5.1.3 Metrics

For the evaluation of results we mainly look at the euclidean distance error between corresponding deformed template \bar{t}_i points and the ground truth s_i^* , i.e. the complete and deformed target shape without noise, averaged over the shape, so $d(s, t) = \frac{1}{N_T} \sum_{i=1}^{N_T} \|s_i^* - \bar{t}_i\|_2^2$. This is then averaged over the entire dataset, consisting of 100 samples. However, it should be noted that BCPD will occasionally not lead to a successful registration, in which case it does not produce an output or does not produce correspondence for any point. Since this result will not be taken into account for the distance metric and often occurs for the most challenging settings, we also present the fraction of successful registration. Our method does not consider a failed registration unless there are no deformations found in the first iteration.

5.1.4 Discussion

The results for all the method and data variations considered can be found in Figure 3. Our main focus is the dataset with increasing missing region (Figure 3a), as this closely replicates the challenges in the ear. While for the lowest level it is evident that BCPD (when optimized) performs better, as we increase the missing area, our method presents a progressive advantage. Comparing *GPReg_Full*, *GPReg_bcpdReg* and *GPReg_noTresh* it becomes clear why those modifications are advantageous when facing extensive missing regions. It is also evident that the closest point approach has the poorest performance overall.

It is also interesting to look at the results in the presence of outliers (Figure 3c and Figure 3d), for which we tested all methods with $\omega = 0.1$ and $\omega = 0.3$ (with the exception of *GPClosestPnt* where this is not applicable), since this parameter reflects the expected outlier probability. While BCPD performs better if this parameter is adequately adjusted to the real outlier occurrence, we note that our method presents almost the same results for both settings. Therefore, if one does not have any prior knowledge on this quantity, our method is more suitable.

Looking at the variation of noise (Figure 3e) and deformations (Figure 3b), we see that overall an adequately set BCPD outperforms our method and is able to achieve lower errors, even when both parameters are previously tuned. We also note that the two variations of our method always perform better than the full proposal for these scenarios — the proposed alterations do not bring an advantage when we are not dealing with structured missing data. However, this decrease in performance is deemed acceptable given the gain it provides in (Figure 3a) and when compared with the Closest Point proposal always leads to lower error.

An intuition of why our method is able to perform well for extensive missing data is offered in Figure 4, where we compare the fitting results from BCPD with different levels of deformation and our proposed method. We can see that the main challenge in achieving an adequate fitting with BCPD is that if we allow for a high level of deformation then the missing region collapses, while in the opposite case the deformations are not enough to fit all details on the non-missing parts. With our approach we are able to avoid collapsing, while allowing enough deformation to fit the fine details.

Furthermore, in Figure 5 we present additional metrics for the missing region version of this dataset. The high performance on both recall and precision for our method tells us that the lower distance error observed before is in fact

coming from an accurate identification of missing points. We notice that the GP with closest point presents a very high precision but at a cost of a low recall.

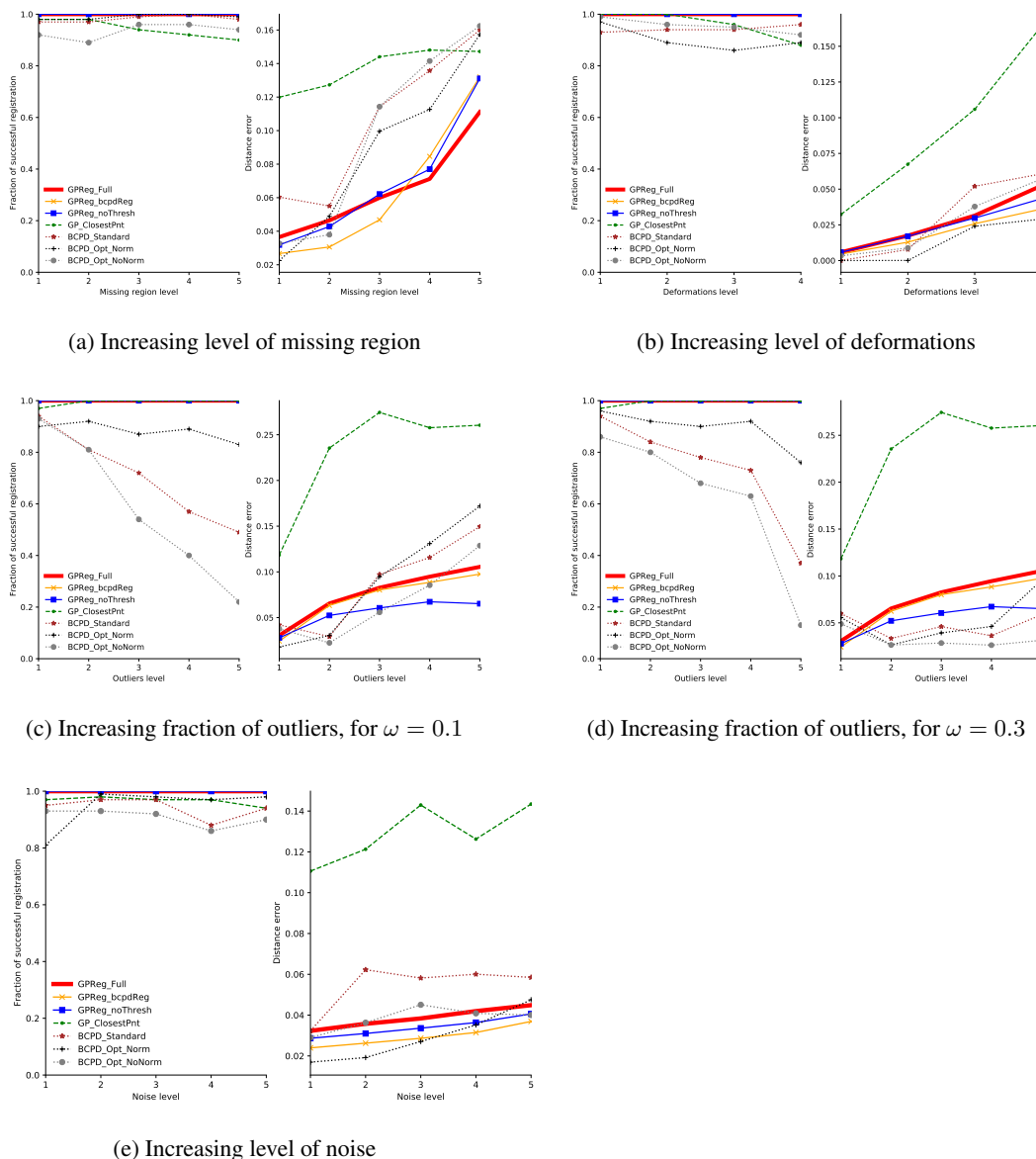


Figure 3: Results for Fish dataset with different types of modifications.

5.2 3D Ear simulated data

5.2.1 Dataset

In this section we test our method with 3D ear data, the main goal of our work. The dataset used is obtained from the Ear dataset in [7], with some subsequent transformations to achieve more realistic shapes, that mimic the real-life challenges observed in true scans (we denote the transformed shapes as Simulated dataset). An example can be found in Figure 1. The employed transformations are described below.

Missing data The real scans have missing points, not only uniformly spread, but also concentrated in particular regions of the ear which are more difficult to capture by the scanning process. Therefore, in the Ear dataset we introduce both uniform and structured missing data points.

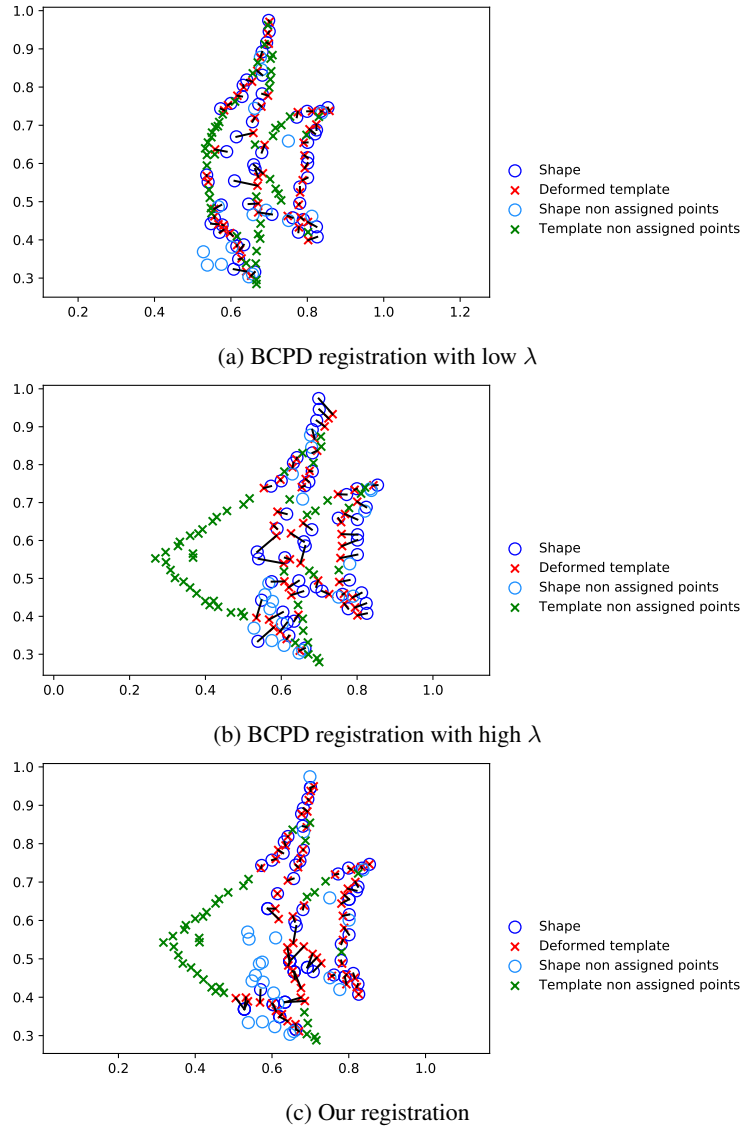


Figure 4: Example for missing data performance with Fish dataset. The target can be seen in blue circles, why the deformed template after registration is represented with red and green crosses. Points with and without correspondence are identified both for the template and target shape. The two results for BCPD are run with different parameter λ responsible for controlling the expected length of the deformation — small values of λ allow for more deformation and vice-versa.

Outliers The ear region also contains outliers (points with no correspondence in the template), both uniformly spread and in a structured manner. In particular, the structured outliers come from the fact that when we cut the ear portion from the entire head of the scan we do not know exactly which points belong to the ear, and consequently include some extra points. Therefore, in the Ear dataset we add both uniform and structured outliers.

Measurement Noise For each point in the Ear dataset we introduce Gaussian noise with zero mean and a chosen variance, so that they are slightly displaced, to simulate the lack of complete accuracy in the screening process.

Slight rotation, translation and scaling Even after removing the main components of these 3 transformations it is expected that the different scans still present a small difference, not only due to limitations on the first step, but also due to natural differences in shape that do not allow for a better result. However, the dataset in [7] is perfectly aligned, which can produce misleading results. Therefore, we subject all shapes to a random rotation, translation and scaling.

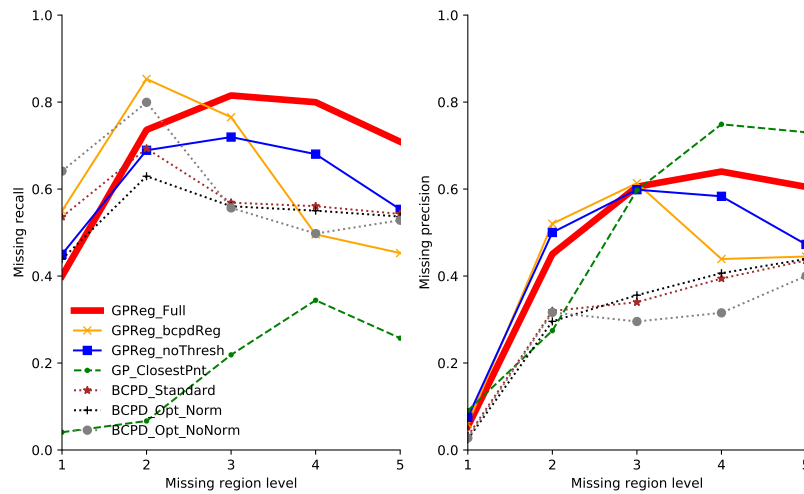


Figure 5: Recall and precision for increasing missing region. A high recall indicates that the methods is able to identify most of the missing points, while a high precision means that most of the points identified as missing are in fact missing.

Furthermore, the dataset and template were subsampled with respect to the original datasets, in order to facilitate computation. We also consider here the fitting of a subset of shapes, as the dataset is composed from 500 samples, but it does not present much variability across them (see our previous work [23] for a more detailed explanation.) Therefore, we consider the shapes with more deformation with respect to the template (measured as the average of Euclidean distance between corresponding shape points).

5.2.2 Discussion

Figure 1 presents the fitting results with both BCPD and GPReg, for the Simulated dataset. For fairness, we consider the GPReg with a Squared Exponential kernel, even if the final goal is to include other information regarding the shape characteristics. We see that even if the non missing point have slight higher error for our method, this is largely compensated by the missing points respective error. In practice, this means that we are less likely to observe unreasonable shapes from the fitting with our method.

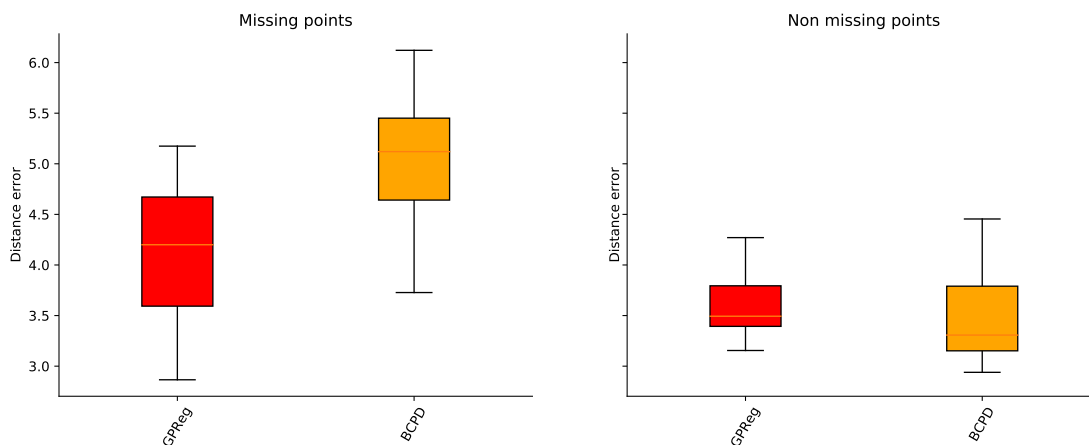


Figure 6: Results for the simulated Ear dataset with GPReg and BCPD. The boxplot is obtained from the mean euclidean distance between the true and deformed template point sets, for all shapes considered.

6 Discussion and future work

We developed a method that bridges the gap between the Gaussian Process framework used in 3D Morphable Models and the probabilistic registration methods, by formulating the shape fitting problem in a GPR multi-annotator setting. This allows us to benefit from advantages on both sides and obtain a method particularly suited for shape fitting in the presence of extensive missing data — a useful tool for challenging shapes such as the human ear.

Naturally, even if the missing points are correctly identified, the shape prediction in those regions will be as good as the prior model. Therefore, it is beneficial to have a more complex and accurate model, able to express more knowledge on the particular shape. As stated, the GP framework offers a very suitable setting, with kernels expressing intuitive properties of the shapes. So, defining a more appropriate kernel is the logical next step. It would also be pertinent to study how the parallel with the probabilistic registration holds when we introduce the missing point set and the threshold, to have a more theoretical insight on the properties of our method.

References

- [1] L. BAI, X. YANG, AND H. GAO, *Nonrigid point set registration by preserving local connectivity*, IEEE Transactions on Cybernetics, 48 (2018), pp. 826–835.
- [2] V. BLANZ AND T. VETTER, *A morphable model for the synthesis of 3D faces*, SIGGRAPH’99 Proceedings of the 26th annual conference on Computer graphics and interactive techniques, (2002).
- [3] D. M. BLEI, A. KUCUKELBIR, AND J. D. MCAULIFFE, *Variational inference: A review for statisticians*, Journal of the American Statistical Association, 112 (2017), p. 859–877.
- [4] J. BOOTH, A. ROUSSOS, S. ZAFEIRIOU, A. PONNIAHY, AND D. DUNAWAY, *A 3D morphable model learnt from 10,000 faces*, in 2016 IEEE Conference on Computer Vision and Pattern Recognition (CVPR), June 2016, pp. 5543–5552.
- [5] A. BRUNTON, A. SALAZAR, T. BOLKART, AND S. WUHRER, *Review of statistical shape spaces for 3D data with comparative analysis for human faces*, Computer Vision and Image Understanding, (2014).
- [6] H. CHUI AND A. RANGARAJAN, *A new algorithm for non-rigid point matching*, in Proceedings IEEE Conference on Computer Vision and Pattern Recognition. CVPR 2000 (Cat. No.PR00662), vol. 2, 2000, pp. 44–51 vol.2.
- [7] H. DAI, N. PEARS, AND W. SMITH, *A data-augmented 3D morphable model of the ear*, in 2018 13th IEEE International Conference on Automatic Face Gesture Recognition (FG 2018), May 2018, pp. 404–408.
- [8] P. GROOT, A. BIRLUTIU, AND T. HESKES, *Learning from multiple annotators with gaussian processes*, in ICANN, 2011.
- [9] M. HEIN AND O. BOUSQUET, *Kernels, associated structures and generalizations*, (2004).
- [10] O. HIROSE, *Acceleration of non-rigid point set registration with downsampling and Gaussian process regression*, IEEE Transactions on Pattern Analysis and Machine Intelligence, 43 (2021), pp. 2858–2865.
- [11] ———, *A bayesian formulation of coherent point drift*, IEEE Transactions on Pattern Analysis and Machine Intelligence, 43 (2021), pp. 2269–2286.
- [12] H. LAGA, *A survey on non-rigid 3d shape analysis*, (2018).
- [13] D. C. LIU AND J. NOCEDAL, *On the limited memory bfgs method for large scale optimization*, Mathematical Programming, 45 (1989), pp. 503–528.
- [14] M. LÜTHI, C. JUD, AND T. VETTER, *A unified approach to shape model fitting and non-rigid registration*, in Proceedings of the 4th International Workshop on Machine Learning in Medical Imaging - Volume 8184, Berlin, Heidelberg, 2013, Springer-Verlag, pp. 66–73.
- [15] M. LÜTHI, T. GERIG, C. JUD, AND T. VETTER, *Gaussian process morphable models*, IEEE Transactions on Pattern Analysis and Machine Intelligence, 40 (2018), pp. 1860–1873.
- [16] J. MA, J. ZHAO, AND A. L. YUILLE, *Non-rigid point set registration by preserving global and local structures*, IEEE Transactions on Image Processing, 25 (2016), pp. 53–64.
- [17] C. MICCHELLI AND M. PONTIL, *On learning vector-valued functions*, Neural computation, 17 (2005), pp. 177–204.
- [18] A. MYRONENKO AND X. SONG, *Point set registration: Coherent point drift*, IEEE Transactions on Pattern Analysis and Machine Intelligence, 32 (2010), pp. 2262–2275.

- [19] P. PAYSAN, R. KNOTHE, B. AMBERG, S. ROMDHANI, AND T. VETTER, *A 3D face model for pose and illumination invariant face recognition*, in 2009 Sixth IEEE International Conference on Advanced Video and Signal Based Surveillance, Sep. 2009, pp. 296–301.
- [20] S. PLOUMPIS, E. VERVERAS, E. O. SULLIVAN, S. MOSCHOGLOU, H. WANG, N. PEARS, W. A. P. SMITH, B. GECER, AND S. ZAFEIRIOU, *Towards a complete 3D morphable model of the human head*, IEEE Transactions on Pattern Analysis and Machine Intelligence, (2020).
- [21] S. PLOUMPIS, H. WANG, N. PEARS, W. A. P. SMITH, AND S. ZAFEIRIOU, *Combining 3D morphable models: A large scale face-and-head model*, in 2019 IEEE/CVF Conference on Computer Vision and Pattern Recognition (CVPR), 2019.
- [22] C. E. RASMUSSEN AND C. K. I. WILLIAMS, *Gaussian Processes for Machine Learning (Adaptive Computation and Machine Learning)*, The MIT Press, 2005.
- [23] F. VALDEIRA, R. FERREIRA, A. MICHELETTI, AND C. SOARES, *From noisy point clouds to complete ear shapes: Unsupervised pipeline*, IEEE Access, PP (2021), pp. 1–1.